



A computational study of the EN 1078 impact test for bicycle helmets using a realistic subject-specific finite element head model

Sandberg, Michael; Tse, Kwong Ming; Tan, Long Bin; Lee, Heow Pueh

Published in:
Computer Methods in Biomechanics and Biomedical Engineering

Link to article, DOI:
[10.1080/10255842.2018.1511775](https://doi.org/10.1080/10255842.2018.1511775)

Publication date:
2018

Document Version
Peer reviewed version

[Link back to DTU Orbit](#)

Citation (APA):
Sandberg, M., Tse, K. M., Tan, L. B., & Lee, H. P. (2018). A computational study of the EN 1078 impact test for bicycle helmets using a realistic subject-specific finite element head model. *Computer Methods in Biomechanics and Biomedical Engineering*, 21(12), 684-692. <https://doi.org/10.1080/10255842.2018.1511775>

General rights

Copyright and moral rights for the publications made accessible in the public portal are retained by the authors and/or other copyright owners and it is a condition of accessing publications that users recognise and abide by the legal requirements associated with these rights.

- Users may download and print one copy of any publication from the public portal for the purpose of private study or research.
- You may not further distribute the material or use it for any profit-making activity or commercial gain
- You may freely distribute the URL identifying the publication in the public portal

If you believe that this document breaches copyright please contact us providing details, and we will remove access to the work immediately and investigate your claim.

1 **A computational study of the EN 1078 impact test for bicycle helmets using a realistic**
2 **subject-specific finite element head model**

3 Michael Sandberg^{1,2*}, Kwong Ming Tse^{1,3*}, Long Bin Tan¹, and Heow Pueh Lee¹

4 *¹Department of Mechanical Engineering, National University of Singapore,*
5 *9 Engineering Drive 1, Singapore 117576;*

6 *²Department of Mechanical Engineering, Technical University of Denmark,*
7 *DK-2800 Kgs. Lyngby, Denmark*

8 *³Department of Mechanical and Product Design Engineering, Swinburne University of*
9 *Technology,*
10 *Advanced Technologies Centre, John St, Hawthorn, Melbourne, VIC 3122, Australia*

11

12 *Corresponding authors:

13 michaelsandberg@mail.com / misan@mek.dtu.dk (Sandberg, M.)

14 tsekm.research@yahoo.com / ktse@swin.edu.au (Tse, K.M.)

15

16 **A computational study of the EN 1078 impact test for bicycle helmets using a realistic**
17 **subject-specific finite element head model**

18 **Abstract**

19 In this paper, the authors aim to establish a numerical framework for computational injury
20 assessment of protective headgear subjected to drop tests. The case study is a bicycle helmet
21 considered in a guided free fall impact test in accordance with the EN 1078 standard for
22 certification of bicycle helmets. A finite element model of a bicycle helmet is created based on
23 generic values for material properties and thicknesses of the helmet layup. The helmet model
24 is coupled to an experimentally validated subject-specific finite element head model. This
25 together constitute the numerical framework, which is found to be adequate by verification
26 against other published results. The impact scenario is simulated with and without a bicycle
27 helmet, and it is demonstrated that the helmet reduces peak resultant translational acceleration,
28 von Mises skull stresses, intracranial pressure, and strain in the brain during the impact.

29 **Keywords:** head injury; bicycle helmet; drop test; biomechanics; crushable foam

30 **1 Introduction**

31 With increasing public awareness of health, fitness, and air pollution, cycling is popular as an
32 alternative to the automobile. In countries like the Netherlands and Denmark, there are
33 approximately 5 million and 1 million cyclists, or about 31% and 19% of the respective
34 population, who prefer bicycles for commutation (European Commission, 2011).
35 Nevertheless, cycling has associated safety risks. Cyclists are generally considered vulnerable
36 road users, whereby a minor misjudgement by a vehicle driver can have significant adverse
37 consequences on a cyclist. As opposed to other modes of commutation, cyclists only have their
38 helmets for protection against fatal injuries in collisions. Therefore, it is particularly important

39 that bicycle helmets follow proven design standards.

40 Bicycle helmet standards generally require that the helmet manufacturers test and qualify their
41 products by performing guided free fall drop tests using artificial headforms. Peak headform
42 accelerations obtained in these tests are then compared against the thresholds prescribed in the
43 standards. For instance, in the United States, the Consumer Product Safety Commission
44 (CPSC, 1998) requires the registered headform peak accelerations to be below 300G for both
45 a 2 m drop (pre-collision velocity of 6.3 m/s) on a flat anvil and 1.2 m drop (4.9 m/s) on
46 hemispheric and curbstone anvils. In Europe, Asia, and South America, the acceleration
47 threshold is 250G for both a 1.5 m drop (5.42 m/s) on a flat anvil and a 1.06 m drop (4.57 m/s)
48 on a kerbstone anvil. Other standards include AS/NZS 2063 (Australia), CAN/CSAD1 13.2-M
49 (Canada) and JIS T 8134 (Japan). Readers are referred to HEADS-ITN (2015) for a
50 comprehensive overview of the current helmet standards.

51 There are currently 28 countries with some form of law for bicycle helmet use (ITF, 2017;
52 European Commission, 2015, 2016; Bicycle Helmet Safety Institute, 2017). Moreover,
53 approximately half of the members of the Organisation for Economic Co-operation and
54 Development (OECD), the International Traffic Safety and Data Analysis Group, and the
55 European Union have some form of bicycle helmet legislation. Wearing a helmet while cycling
56 has been proven as an effective way to mitigate head injuries in relation to collisions (bicycle
57 crashes or falls). Using headform impact tests, Cripton et al. (2014) showed that in a collision
58 at 6.3 m/s and 5.42 m/s, severe brain injury is extremely likely to occur, with 99.9% probability
59 based on the head injury criterion (HIC). However, these probabilities were reduced to 30.6%
60 and 9.3% respectively, for the two impact velocities, when a bicycle helmet is worn. A similar
61 study was published by McIntosh et al. (2013), who conducted impact tests with impact speeds
62 of up to 6.9 m/s in several different impact orientations and locations. Here it was concluded

63 that helmet use was the most significant factor in reducing the probability of head injury. The
64 effect has also been documented through epidemiological studies. Olivier and Creighton
65 (2017) recently completed the largest ever systematic review and meta-analysis by collecting
66 data from 40 different studies from USA, Europe, Australia and Asia. With data based on more
67 than 64,000 injured cyclists, it was concluded that “helmet use is associated with odds
68 reductions of 51% for head injury, 69% for serious head injury, 33% for face injury and 65%
69 for fatal head injury”.

70 In addition to the aforementioned experimental and retrospective studies, computer
71 simulations, such as the finite element (FE) method, provides an alternative to experimental
72 methods in estimating the biomechanical responses of the human head. For example, the effect
73 of utilising a bicycle helmet has been demonstrated with FE simulations of three different
74 impact scenarios in Fahlsted (2016)’s study. This study showed that the risks of skull fracture
75 and concussion were reduced by up to 98% and 46%, respectively, by wearing a helmet.
76 Computer simulations for design and optimisation of protective headgear is also an active
77 research field. Potentially, with the growing knowledge about head injuries and capabilities of
78 modern computers, the level of protection can be accessed and analysed using FE simulations.
79 For instance, Mills and Gilchrist (2008) employed a validated FE model of a commercially
80 available bicycle helmet to investigate the effect of friction between the helmet shell and road
81 surface on peak head acceleration in oblique impacts. The effect of foam liner material
82 properties has been investigated by Asiminei et al. (2009), who varied both the density and
83 modulus of the protective foam (expanded polystyrene, EPS). Teng et al. (2013) studied the
84 effect of IMPAXX foam on head impact accelerations, as an alternative to the most commonly
85 used foam type in bicycle helmets (EPS). As outlined, previous research has focused primarily
86 on the helmet materials as well as helmet liners, but limited attention has been paid on head
87 injury assessment. Moreover, many of these computational studies have used oversimplified

88 FE head models or artificial headforms for the head impact analyses which neither provide
89 insights to the injury mechanics within the brain nor detail the brain regions which could be
90 most affected by the impact.

91 The current study employs an anatomically detailed and experimentally verified subject-
92 specific head model to simulate the particular impact prescribed by the helmet standard EN
93 1078 for Europe, Asia, and South America. This computational approach does not only provide
94 an alternative to experimental helmeted drop tests used in bicycle helmet test standards, but
95 also allows injury assessment and evaluation of the intracranial biomechanical injury metrics,
96 such as intracranial pressure (ICP) and strains, which cannot be determined using the headform
97 or simplified FE head models, in these dynamic events. Finally, this study also investigates the
98 effectiveness of a bicycle helmet in protecting our heads.

99 **2 Methods and materials**

100 ***2.1 Head model***

101 Geometrical information of the human skull and brain were obtained from high resolution axial
102 computed tomography (CT) and magnetic resonance imaging (MRI) images of a 51-year-old
103 Caucasian male subject respectively. These medical images were imported into Mimics v13.0-
104 v14.0 (Materialise, Leuven, Belgium) for the segmentation and reconstruction of the FE human
105 head model, which comprises the skeletal skull, nasal septal cartilage, nasal lateral cartilage,
106 with the overlying soft tissue, the cerebrospinal fluid (CSF), the white and grey matters of
107 cerebrum, cerebellum, the ventricular system, the midbrain, the brainstem as well as the air-
108 containing sinuses. Various components of the head model can be seen in Figure 1. All the
109 skeletal tissues such as cartilages and cervical vertebrae were modelled as linear elastic,
110 isotropic materials while the brain tissues were assumed to be linear viscoelastic. The material
111 properties of the various components of the FE head model can be found in Table 1 and Tse et

112 al. (2014). It should also be noted that the FE head model was validated against the ICP and
113 relative displacement data of three cadaveric experiments (Nahum et al. 1977; Trosseille et al.,
114 1992; Hardy, et al., 2001). More details on the development and validation of the FE head
115 model can be found in Tse et al. (2014).

116 [Figure 1 around here]

117 [Figure 2 around here]

118 [Table 1 around here]

119 **2.2 Bicycle helmet model**

120 The FE model of the bicycle helmet was constructed based on geometry and thicknesses of a
121 generic bicycle helmet layup. In addition, common helmet features such as ventilation holes
122 and retention straps were incorporated in the helmet FE model (Figure 2). The full breakdown
123 of properties and element types are listed in Table 1.

124 The bicycle helmet consists of five parts: (i) An energy absorbing EPS foam partly covered by
125 (ii) a polycarbonate (PC) shell, with (iii) retention straps, (iv) cushion pads, and (v) a fixture to
126 fit the helmet to the head model. All the components of the bicycle helmet, besides the EPS
127 foam, were considered to be isotropic and linear elastic, and their material properties were
128 taken from previously reported studies (Teng et al., 2013; van den Bosch, 2006; Tan et al.,
129 2012) as shown in Table 1. Following the modelling approaches adopted by Mills and Gilchrist
130 (2008) and Milne et al. (2012, 2014), the crushable foam plasticity model in AbaqusTM
131 (Dassault Systemes, 2013) was used to mimic the EPS foam in this study. In addition, the
132 crushable foam model employed in the study was validated experimentally by Cui et al. (2009)
133 for EPS under impact loads. The constitutive law of this closed cell foam can be described in

134 three stages:

135 (i) In the first stage, the material response is linear elastic until the stress state reaches the
136 yield stress.

137 (ii) In the second stage, the material reaches a plateau level where it continues to deform
138 under an almost constant stress state. This corresponds to the level where most of the
139 energy is absorbed as the foam cells collapse.

140 (iii) In the final stage, all foam cells have collapsed, and the material response is again
141 linear elastic.

142 This constitutive law is shown in Figure 3 for the plastic range. According to Dassault Systemes
143 (2013), the yield surface, which is shaped like an ellipse, is described by the following
144 equations (1):

$$145 \sqrt{\sigma_Y + \alpha(p - p_0)^2} - B = 0, \text{ with } p_0 = \frac{p_c - p_t}{2}, \quad B = \alpha \frac{p_c + p_t}{2}, \quad \alpha = \frac{3k}{(3k_t + k)(3 - k)} \quad (1)$$

146 where σ_Y is the Von-Mises stress, p is the hydrostatic pressure, p_c and p_t are the yield strengths
147 of the material in hydrostatic compression and tension, respectively. k describes the ratio
148 between the initial yield stress in uniaxial compression and initial yield stress in hydrostatic
149 compression, and k_t is the ratio between yield strength in hydrostatic tension and initial yield
150 stress in hydrostatic compression. These values, k and k_t , were set to 0.1 and 1.933 (Table 1),
151 respectively, according to Cui et al. (2009), Mills and Gilchrist (2008), and Dassault Systemes
152 (2013).

153 [Figure 3 around here]

154 **2.3 Numerical replication of the EN 1078 standard (contact, boundary conditions, and**
155 **loading)**

156 According to the EN 1078 standard, the “to be qualified” helmet equipped with the testing
157 headform undergoes a guided free fall either using a twin wire or monorail test rig onto a flat
158 anvil fixed on a rigid base. In our simulations, an initial velocity of 5.42 m/s corresponding to
159 the final velocity before impact for an object subjected to gravity ($G \equiv 9.81 \text{ m/s}^2$), was applied
160 to the model, before impacting a fixed anvil (Figure 4). All the nodes at the bottom of the anvil
161 were assigned fixed boundary conditions. The entire simulated impact was captured in 6 ms. It
162 should be noted that the pretension in the retention straps of the bicycle helmet was accounted
163 for in an initial step of the simulations prior to the impact, with a preloading of approximately
164 5 N in each strap according to Mills and Gilchrist (2008).

165 The interaction between intracranial contents (skull and CSF, CSF and brain tissues as well as
166 self-interaction of intracranial brain tissues) were represented by normal pressure-overclosure
167 and tangential sliding contact definitions, with the coefficient of friction of 0.2 (Kleiven and
168 Hardy, 2002; Willinger et al., 1995; Zhang et al., 2001), while the other extracranial bony and
169 cartilaginous components are fused together. For the interfaces between the helmet and head,
170 and helmet and anvil, contact was defined using a penalty formulation for tangential behaviour
171 with kinetic friction. A kinetic friction coefficient of 0.2 was applied between the head and
172 helmet, and a coefficient of 0.1 between the helmet and anvil in accordance with Milne et al.
173 (2012). Similar to the modelling approaches adopted by Mills and Gilchrist (2008) and Milne
174 et al. (2012, 2014), all the interfaces between different components of the helmet were meshed
175 in such a way that they share common nodes with their adjacent interfaces. This technique is
176 beneficial in terms of reducing computation time and is considered acceptable as no or very
177 little relative motion between individual helmet components is expected. This implies that the

178 adhesion between components is considered to remain intact during the impact, meaning the
179 collapsible EPS foam is the only helmet component that will absorb energy through irreversible
180 deformation.

181 ***2.4 Evaluation of head kinematic response and injury metrics***

182 The kinematic response of the head undergoing the impact was evaluated by its translational
183 accelerations. These were calculated as mean values of the ten nodes nearest the centre of
184 gravity of the head (marked as CG in Figure 1). For assessment of skull and brain injuries,
185 three biomechanical metrics were evaluated to analyse the post-processed transient brain
186 response. *Intracranial Strains*: Maximum principal strains were used as a measure of diffuse
187 axonal injury (DAI). Morrison et al. (2003)'s in vitro tests of living brain tissue showed that a
188 mechanical deformation with a positive principal strain exceeding 0.2 led to cell damage and
189 death, and thus consequently DAI. *Intracranial Pressure (ICP)*: ICP has been hypothesised to
190 be one of the most critical biomechanical injury metrics in traumatic brain injury (TBI) since
191 an elevated ICP in head trauma can lead to severe brain damage (Tse et al., 2017). An ICP
192 injury criterion, proposed by Ward et al. (1980) based on combined numerical and
193 experimental investigation of live animals and human cadavers, states that serious or fatal brain
194 injury occurs when the peak ICP exceeds 0.235 MPa, while no or minor brain injury occurs
195 when the ICP is below 0.173 MPa. *Von Mises skull stress*: The critical failure level for the
196 human skull is approximated by a von Mises stress threshold of 75 MPa, which is based on the
197 average of the reported range from McElhaney et al. (1970)'s mechanical experiments
198 conducted on human skull samples.

199 **3. Results and discussion**

200 Figure 4 shows the transient accelerations measured at the CG of the head, while Figure 5

201 illustrates the contour plots of the ICP and principal true strain for the brain, as well as the von
202 Mises stresses of the skull at various time instants during the impact. The peak values are listed
203 in Table 3.

204 [Figure 4 around here]

205 [Figure 5 around here]

206 [Table 3 around here]

207 ***3.1 Verification of the helmet model and numerical framework***

208 The peak translational acceleration and impact duration obtained in the current work were
209 benchmarked against Milne et al. (2012)'s and Fahlstedt et al. (2016)'s FE modelling studies,
210 which reported values for the same impact scenario in accordance with the EN 1078 standard.
211 The comparison of the value of these parameters between the present work and the two
212 aforementioned studies is presented in Table 2.

213 The predicted maximum head acceleration was found to be 223G, which was approximately
214 28% and 1% higher than the values in Milne et al. (2012)'s and Fahlstedt et al. (2016)'s studies,
215 respectively. As for the impulse duration, our simulation predicted that the impact generated
216 an impulse lasting for 5 ms, while the respective impulse durations in Milne et al. (2012)'s and
217 Fahlstedt et al. (2016)'s simulations were approximately 3 ms and 1 ms longer. The predictions
218 presented in the current study are in good agreement with those values reported by Fahlstedt et
219 al. (2016), even though the peak resultant translational acceleration appears to be overestimated
220 and the impact duration to be underestimated when compared to Milne et al. (2012)'s
221 simulations. These slight differences or discrepancy with Milne et al. (2012)'s study are
222 justifiable due to the different head masses used in these simulations. As shown in Table 2, the

223 heavier head model used in Milne et al. (2012)'s simulation is expected to result in a more
224 gradual velocity reversal, and thus a lower acceleration due to mass inertia effect. Moreover,
225 our predicted peak head acceleration was also found to be within the 250 G threshold given by
226 EN 1078 standard for direct impact, which implied that the helmet model adequately
227 exemplifies a general bicycle helmet designed according to the EN 1078 standard.

228 [Table 2 around here]

229 ***3.2 Injury assessment using biomechanical metrics***

230 A peak in von Mises skull stress of 85 MPa was obtained at the impact site, shortly after the
231 impact, as shown in Figure 5 and Table 3. This level is above the 75 MPa criterion based on
232 McElhaney et al. (1970), which implies that the impact will result in a skull fracture. When
233 wearing a helmet, the peak von Mises skull stress was reduced to approximately 10 MPa, which
234 corresponds to a reduction of 88%. As this level was well below the failure limit of 75 MPa,
235 this demonstrates that the bicycle helmet is effective in preventing skull fracture for this
236 particular impact condition.

237 The maximum principal true strain of the brain occurred after the peak in von Mises stress of
238 the skull, due to a natural delay for the motion of the softer viscoelastic brain. The region near
239 the impact zone at the parietal skull bone experienced relative high strains of about 0.8, which
240 was reduced to 0.7 (-13%) by equipping with a helmet. As shown in Figure 5, there were large
241 areas of the brain exceeding Morrison et al. (2003)'s strain injury threshold of 0.2 during the
242 simulated impact duration. This indicates that there is a significant risk of DAI in both impact
243 scenarios, which is however reduced when a helmet is worn as the strain levels are lower.

244 The intracranial pressure (ICP) response behaved similarly as the brain principal strains. The
245 maximum positive ICP, at 0.65 MPa, was observed in regions close to the impact zone mainly

246 in the grey matter, which was reduced to 0.45 MPa (31%) when a helmet was helmet worn.
247 Both impacts resulted in values that exceeded Ward et al. (1980) ICP threshold of 0.235 MPa,
248 but again a significant reduction was observed when the head model was equipped with the
249 helmet.

250 **3.3 Limitations**

251 A key limitation of this study was that the intracranial transient responses, which are the basis
252 for injury assessment using the proposed injury metrics, are not only dependent on the physical
253 parameters employed, but also the interaction properties and constraints enforced in the model.
254 As it appears in Figure 5, relative deformation occurred between the intracranial components
255 of the head. In particular, intermittent gaps develop in interfaces between the skull and CSF,
256 and the CSF and white matter during the impact. These are the potential locations for negative
257 ICP which could also be an important biomechanical injury metric, but could also be caused
258 by limitations of the model.

259 The pulsatile cerebrospinal fluid (CSF) was assumed linear elastic for the head model, which
260 is a normal, necessary assumption for head models with this level of complexity. One cannot
261 resort to computationally intensive fluid-structure interaction simulations, and this is usually
262 acceptable due to limited relative motion between the brain components. Furthermore, the
263 components in the current head model were unconstrained, except for the contact property
264 between them which restrained penetration. In reality, the various head components are
265 connected by different nerves, which restrict their relative motion to some extent. The
266 discretionary use of different types of contact interactions or constraints would affect the
267 simulation results, as also noted and reported by Bar-Kochba et al. (2012), but addressing this
268 issue is complex since there is limited in-vivo human head test data to reveal the actual contact
269 interaction properties between the various components.

270 Smaller regions of high ICPs and strains were observed in the brain during the impact as seen
271 in Figure 5. When using a penalty contact formulation, penetration is avoided by upholding a
272 restoring, coupling force between components. As for this relatively complex geometry of the
273 brain and these large deformations, many local areas with high pressure can arise from these
274 contact forces. This phenomenon was not reported by Milne et al. (2012) who employed a
275 relatively simplified FE head model, in which the convoluted topography of the brain was
276 idealised as a smooth surface.

277 **4. Conclusion**

278 In the current study, an enhanced, anatomically detailed and experimentally verified subject-
279 specific head model, coupled with a bicycle helmet model was used to simulate the test impact
280 as prescribed by the helmet standard EN 1078 for Europe, Asia, and South America. Using the
281 simulation model, it was demonstrated how the peak resultant translational acceleration was
282 reduced by 75%, the von Mises skull stress by 88%, the ICP by 31%, and the max. principal
283 strain in the brain by 15% when the model was wearing a bicycle helmet in the test impact. It
284 is anticipated that the presented numerical model can be used in the future to go beyond the
285 enforced test standards in terms of evaluating and optimising helmet designs by analysing
286 multiple and more complex injury scenarios.

287

288 ***3609 words***

289 **Conflicts of interest**

290 None

291 **Acknowledgments**

292 The first author would like to acknowledge the fruitful discussions and help he received from
293 staff and students during his research stay at Applied Mechanics Laboratory, National
294 University of Singapore.

295 **References**

- 296 Asiminei, A. G., Goffin, J., Van Der Perre, G., & Verpoest, I. (2009). A transient finite element
297 study reveals the importance of the bicycle helmet material properties on head protection
298 during an impact. *International Research Council on the Biomechanics of Injury - 2009*
299 *International IRCOBI Conference on the Biomechanics of Injury, Proceedings*, 357–360.
- 300 Bar-Kochba, E., Gutttag, M., Sett, S., Franck, J. A., McNamara, K., Crisco, J., & Franck, C.
301 (2012). Finite Element Analysis of Head Impact in Contact Sports. In *SIMULIA*
302 *Community Conference (SCC)* (p. 10).
- 303 Bicycle Helmet Safety Institute (2017). Bicycle Helmet Laws. Available at
304 <https://helmets.org/mandator.htm>.
- 305 Cui, L., Kiernan, S., & Gilchrist, M. D. (2009). Designing the energy absorption capacity of
306 functionally graded foam materials. *Materials Science and Engineering: A*, 507(1), 215-
307 225.
- 308 CPSC (1998), Consumer Product Safety Commission, Safety Standard for Bicycle Helmets;
309 Final Rule, USA
- 310 Cripton, P. A., Dressler, D. M., Stuart, C. A., Dennison, C. R., & Richards, D. (2014). Bicycle
311 helmets are highly effective at preventing head injury during head impact: Head-form
312 accelerations and injury criteria for helmeted and unhelmeted impacts. *Accident Analysis*
313 *& Prevention*, 70, 1-7.
- 314 Dassault Systmes (2013), ABAQUS User's Manual 6.13, Dassault Systmes, USA

315 European Commission (2011), The Gallup Organisation, Future of transport - Analytical
316 report, Europe

317 European Commission (2015). Road safety in the European Union; Trends, statistics and main
318 challenges, European Union

319 European Commission (2016) Road safety in the European Union; Trends, statistics and main
320 challenges, European Union

321 European standard (1997), EN 1078, Helmets for pedal cyclists and for users of skateboards
322 and roller skates

323 Kleiven, S., & Hardy, W. N. (2002). Correlation of an FE Model of the Human Head with
324 Local Brain Motion--Consequences for Injury Prediction. *Stapp Car Crash Journal*, (46),
325 123-44.

326 Fahlstedt, M., Halldin, P., & Kleiven, S. (2016). The protective effect of a helmet in three
327 bicycle accidents—A finite element study. *Accident Analysis & Prevention*, 91, 135-143.

328 Hardy WN, Foster C, Mason M, Yang K, King A, Tashman S. Investigation of head injury
329 mechanisms using neutral density technology and high-speed biplanar x-ray. *45th Stapp*
330 *Car Crash Conference*, San Antonio, USA, 2001; 337–368.

331 HEADS-ITN (2015). *Current Standards for Sports and Automotive Helmets: A Review.*,
332 Available at http://www.heads-itn.eu/pdfs/Helmets_Standard_Evaluation.pdf (Section
333 2.1)

334 ITF (2017). Road Safety Annual Report 2017, OECD Publishing, Paris.

335 McElhaney, J. H., Fogle, J. L., Melvin, J. W., Haynes, R. R., Roberts, V. L., & Alem, N. M.
336 (1970). Mechanical properties of cranial bone. *Journal of biomechanics*, 3(5), 495-511.

337 McIntosh, A. S., Lai, A., & Schilter, E. (2013). Bicycle helmets: head impact dynamics in
338 helmeted and unhelmeted oblique impact tests. *Traffic injury prevention*, 14(5), 501-508.

339 Morrison III, B., Cater, H. L., Wang, C. C., & Thomas, F. C. (2003). A tissue level tolerance
340 criterion for living brain developed with an in vitro model of traumatic mechanical loading.
341 *Stapp Car Crash Journal*, 47, 93.

342 Mills, N. J., & Gilchrist, A. (2008). Finite-element analysis of bicycle helmet oblique impacts.
343 *International Journal of Impact Engineering*, 35(9), 1087-1101.

344 Milne, G., Deck, C., Carreira, R. P., Allinne, Q., & Willinger, R. (2012). Development and
345 validation of a bicycle helmet: Assessment of head injury risk under standard impact
346 conditions. *Computer methods in biomechanics and biomedical engineering*, 15(1), 309-
347 310.

348 Milne, G., Deck, C., Bourdet, N., Carreira, R. P., Allinne, Q., Gallego, A., & Willinger, R.
349 (2014). Bicycle helmet modelling and validation under linear and tangential impacts.
350 *International Journal of Crashworthiness*, 19(4), 323-333.

351 Nahum AM, Smith R, Ward CC. Intracranial pressure dynamics during head impact. In *21st*
352 *Stapp Car Crash Conference. Society of Automotive Engineers (SAE)*, SAE Paper No.
353 770922: San Diego, USA, 1977; 339–366.

354 Newman, J. A., Shewchenko, N., & Welbourne, E. (2000). A proposed new biomechanical
355 head injury assessment function-the maximum power index. *Stapp car crash journal*, 44,
356 215-247.

357 Olivier, J., & Creighton, P. (2016). Bicycle injuries and helmet use: a systematic review and
358 meta-analysis. *International journal of epidemiology*, 46(1), 278-292.

359 Schaller, A., Voigt, C., Huempfer-Hierl, H., Hemprich, A., & Hierl, T. (2012). Transient finite
360 element analysis of a traumatic fracture of the zygomatic bone caused by a head collision.
361 *International journal of oral and maxillofacial surgery*, 41(1), 66-73.

362 Takhounts, E. G., Eppinger, R. H., Campbell, J. Q., & Tannous, R. E. (2003). On the
363 development of the SIMon finite element head model. *Stapp car crash journal*, 47, 107.

364 Tan, L. B., Tse, K. M., Lee, H. P., Tan, V. B. C., & Lim, S. P. (2012). Performance of an
365 advanced combat helmet with different interior cushioning systems in ballistic impact:
366 Experiments and finite element simulations. *International Journal of Impact Engineering*,
367 50, 99-112.

368 Teng, T. L., Liang, C. L., & Nguyen, V. H. (2013). Development and validation of finite
369 element model of helmet impact test. Proceedings of the Institution of Mechanical
370 Engineers, *Part L: Journal of Materials Design and Applications*, 227(1), 82-88.

371 Trosseille X, Tarriere C, Lavaste F. Development of a FEM of the human head according to a
372 specific test protocol. In *30th Stapp Car Crash Conference. Society of Automotive*
373 *Engineers (SAE)*, SAE Paper No. 922527: Warrendale, USA, 1992; 235–253.

374 Tse, K. M., Tan, L. B. and Lee, H. P. (2017). Chapter 10: The Skull and Brain: Computer
375 models for the head and its protection. In Franklyn, M. and Lee, P. V. S. (eds) *Military*
376 *Injury Biomechanics: The Cause and Prevention of Impact Injuries*: CRC Press, pp. 175-
377 220.

378 Tse, K. M., Tan, L. B., Lim, S. P., & Lee, H. P. (2015). Conventional and complex modal
379 analyses of a finite element model of human head and neck. *Computer methods in*
380 *biomechanics and biomedical engineering*, 18(9), 961-973.

381 Tse, K. M., Tan, L. B., Lee, S. J., Lim, S. P., & Lee, H. P. (2014). Development and validation
382 of two subject-specific finite element models of human head against three cadaveric
383 experiments. *International journal for numerical methods in biomedical engineering*,
384 30(3), 397-415.

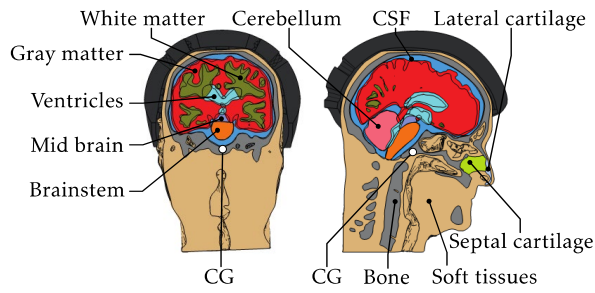
385 E. van den Bosch (2006), "Crash Helmet Testing and Design Specifications", Ph.D. thesis,
386 Eindhoven University of Technology, Department of Mechanical Engineering, Section of
387 Dynamics and Biomechanics.

388 Ward, C., Chan, M., & Nahum, A. (1980). Intracranial pressure—a brain injury criterion (No.
389 801304). SAE Technical Paper.

390 Willinger, R., Taleb, L., & Kopp, C. M. (1995). Modal and temporal analysis of head
391 mathematical models. *Journal of neurotrauma*, 12(4), 743-754.

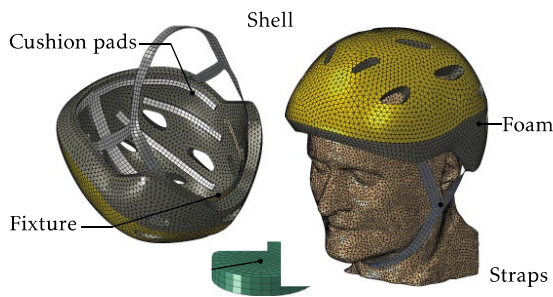
392 Zhang, L., Yang, K. H., & King, A. I. (2004). Comparison of brain responses between frontal
393 and lateral impacts by finite element modeling. *Journal of neurotrauma*, 18(1), 21-30.

394



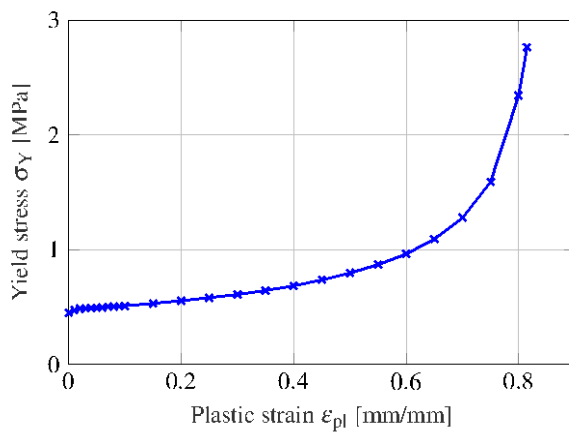
395

396 Figure 1: Frontal and sagittal view of head model, and probe location (CG).



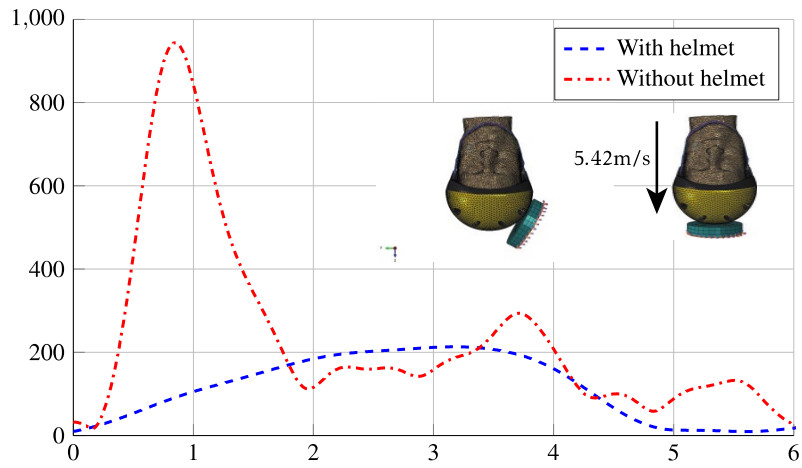
397

398 Figure 2: Mesh of bicycle helmet model, anvil and the assembled helmet-head model with
 399 orientation of the coordinate system.



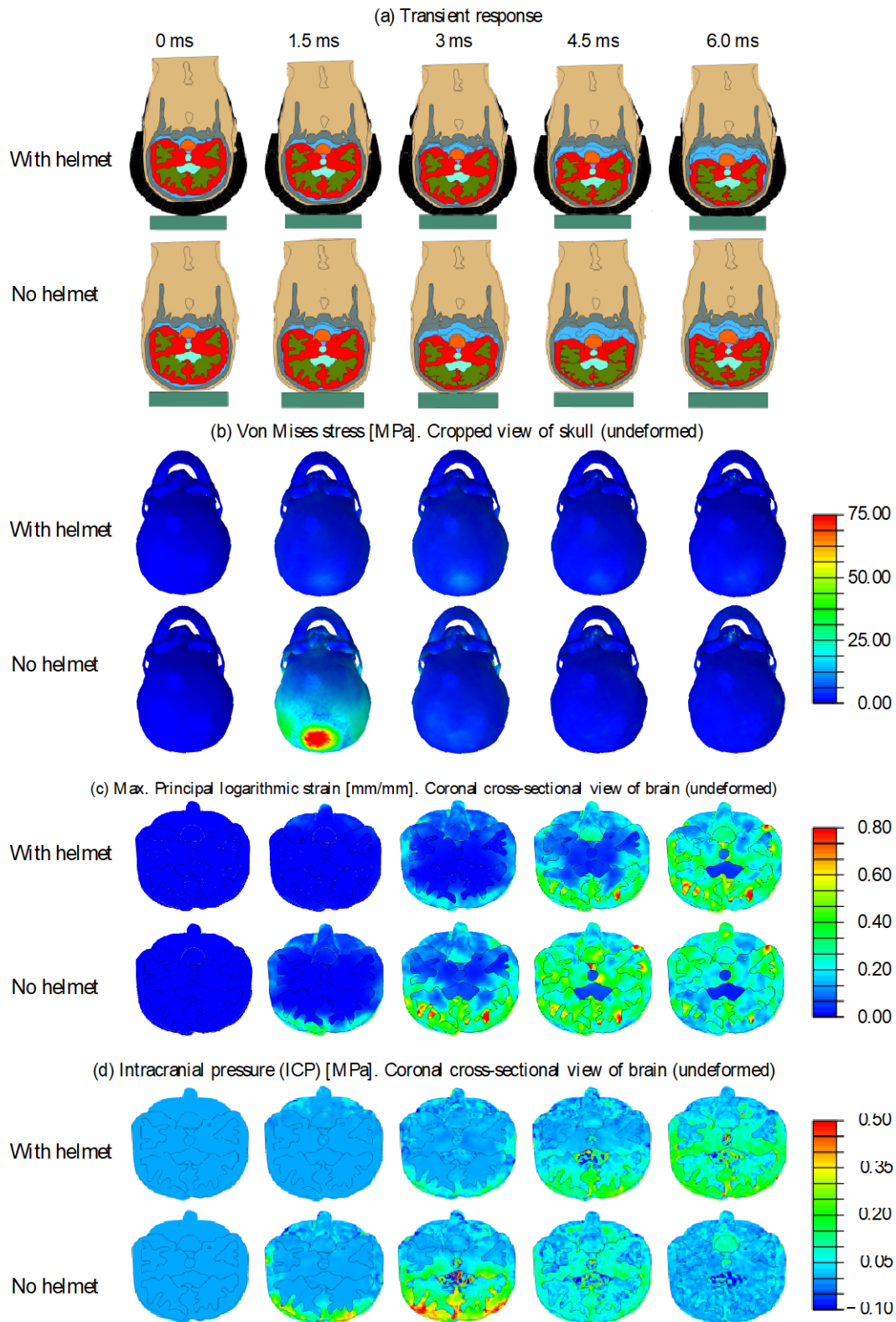
400

401 Figure 3: Constitutive relation (Yield stress/plastic strain) of the expanded polystyrene (EPS)
 402 foam.



403

404 Figure 4: Resulting translational acceleration at CG of the headform for the EN 1078 impact,
 405 equivalent to a 1.5 m guided free fall.



406

407 Figure 5: Resulting field variables for the EN 1078 impact: Guided 1.5 m direct free fall on
 408 flat anvil. (a) Transient response, (b) Von mises stress, (c) Principal logarithmic strain, and
 409 (d) Intracranial pressure.

410

Components of the helmet	No. and types of elements *	Thickness [mm]	Elasticity [MPa]	Poisson's ratio [-]	Density [kg×mm ⁻³]	References
EPS Foam [#]	48,416 C3D4	20	E = 20; $\sigma_Y = 0.140$; k = 0.1; $k_t = 1.933$	-	0.064×10^{-6}	Dassault Systmes (2013); Cui et al. (2009); Mills and Gilchrist (2008)
Cushion pads	1,632 C3D4	3	E = 0.47	-	0.032×10^{-6}	Teng et al. (2013)
Shell	4,116 S3R	0.4	E = 15	0.42	1.5×10^{-6}	van den Bosch (2006)
Fixture	128 S4R	1.5	E = 2	0.35	1.5×10^{-6}	
Straps	342 S4R	1.5	E = 0.06	0.25	0.4×10^{-6}	Tan et al. (2012)
<i>Total, helmet: 54,000 elements, 0.194 kg</i>						
Components of the test setup	No. and types of elements *	Thickness [mm]	Elasticity [MPa]	Poisson's ratio [-]	Density [kg×mm ⁻³]	References
Anvil	576 C3D8R	24	E = 200	0.25	7.8×10^{-6}	European standard (1997)
<i>Total, anvil: 576 elements, 2.32 kg</i>						
Components of the head	No. and types of elements *	Elasticity / Viscoelasticity [MPa] $G(t) = G_\infty + (G_0 - G_\infty)e^{-\beta t}$ with $G_{0,\infty}$ [MPa], β [s ⁻¹])		Poisson's ratio [-]	Density [kg×mm ⁻³]	References
Brainstem [^]	6,104 C3D4	$G_0 = 0.0225$, $G_\infty = 0.0045$, $\beta = 80$		0.4996	1.06×10^{-6}	Tse et al. (2014)
Cerebral peduncle [^]	1,762 C3D4	$G_0 = 0.0225$, $G_\infty = 0.0045$, $\beta = 80$		0.4996	1.06×10^{-6}	Tse et al. (2014)
CSF	164,864 C3D4	E = 1.314		0.4999	1.04×10^{-6}	Tse et al. (2014)
Grey matter [^]	436,917 C3D4	$G_0 = 0.034$, $G_\infty = 0.0064$, $\beta = 700$		0.4996	1.04×10^{-6}	Tse et al. (2014)
Lateral cartilage	2,874 C3D4	E = 30		0.45	1.50×10^{-6}	Tse et al. (2014)
Septum cartilage	3,578 C3D4	E = 9		0.32	1.50×10^{-6}	Tse et al. (2014)
Bone	130,482 C3D4	E = 8000		0.22	1.21×10^{-6}	Tse et al. (2014)
Soft tissues	253,894 C3D4	E = 16.7		0.46	1.04×10^{-6}	Tse et al. (2014)
Ventricles	36,776 C3D4	E = 1.314		0.4999	1.04×10^{-6}	Tse et al. (2014)
White matter [^]	278,925 C3D4	$G_0 = 0.034$, $G_\infty = 0.0064$, $\beta = 700$		0.4996	1.04×10^{-6}	Tse et al. (2014)
<i>Total, head: 1,300,000 elements, 4.73 kg</i>						

[#] with material non-linearity, volumetric hardening

[^] with material non-linearity, viscoelasticity, where G_∞ is the long-term shear modulus, G_0 is the short term shear modulus, and β is the decay factor

* C3D4 refers to solid tetrahedral and C3D8R refers to solid hexahedral elements. S3R and S4R are reduced-integration triangular and quadrilateral shell elements, respectively.

411

412 Table 1: Mechanical properties for the different components. If not otherwise stated,

413 components are considered isotropic and linear-elastic.

Reference	Head model	Peak resultant linear acceleration	Impact duration
The current study	Tse et al. (2014), 4.73 kg	223G	5ms
Milne et al. (2012)	Strasbourg University Finite Element Head Model, 5.7 kg	174G	8ms
Fahlstedt et al. (2016)	Hybrid III dummy head, 4.54 kg	220G	6ms

414

415 Table 2: Benchmarks for model validation.

Field variable	Without helmet	With helmet	Reduction
Peak resultant linear acceleration	944G	223G	75%
Von Mises stress in skull	85 MPa (*1.2ms)	10 MPa (3.6ms)	88%
Max. Intracranial pressure (ICP) in brain	0.65 MPa (3.4ms)	0.45 MPa (5.3ms)	31%
Max. Principal strain in brain	0.8 [-] (3.4ms)	0.7 [-] (5.4ms)	15%

(* all parentheses hold the time of the occurrence)

416

417 Table 3: Peak values of acceleration and field variables, incl. reductions.